Active Pitch Links and Trailing-Edge Tabs for Rotor Track and Balance

Jayanth Krishnamurthi
Graduate Research Assistant
Rensselaer Polytechnic Institute
Troy, NY, USA

Farhan Gandhi
Redfern Professor of Aerospace Engineering
Rensselaer Polytechnic Institute
Troy, NY, USA

ABSTRACT

This study compares the effectiveness of an on-blade active trailing-edge tab and an adjustable pitch link mechanism for rotor track-and-balance. The active tab is an extendable trailing-edge-plate over a spanwise section of each blade. A simulation model of the UH-60 Black Hawk rotor with seeded imbalance is developed, with the pitch links/tabs minimizing the 1/rev (1P) vibratory loads using a weighted least-squares optimization method. The trailing-edge tab has the ability to significantly reduce the 1P in-plane forces in hover but shows more modest reductions in cruise. The tabs are unable to reduce 1P vertical forces in hover but are very effective in reducing them in cruise, and are also moderately effective in reducing 1P in-plane moments over the range of airspeeds. Best reductions in 1P loads are achieved by employing an active tab mechanism (adjusted at different airspeeds) over a passive mechanism (with constant setting over the airspeed range), with the active tab yielding additional gains in 1P in-plane forces and moments in hover and in 1P vertical forces in cruise. Compared to the trailing-edge tab, the pitch link shows significantly larger reductions in 1P in-plane forces over all airspeeds and simultaneously reduces 1P vertical force to comparable levels in cruise. Reductions in 1P in-plane moments with the pitch link are comparable to those with the trailing-edge tabs in hover but show a slight improvement in cruise. In contrast to the trailing-edge tab, minimal differences are observed between active and passive pitch links, except for the case of 1P in-plane forces in hover. In hover, for both tab and pitch link, an examination of the load reduction process indicates that a seeded radial shear and root torsional moment imbalance is cancelled by the generation of net blade root chordwise shear and root flap bending moments, respectively, on orthogonal blades. In cruise, a similar process is observed, but the generation of net radial shears and root torsional moments on opposing blades were also contributors to total reduction in 1P hub in-plane and pitching moment vibrations for the trailing-edge tab.

NOMENCLATURE

c	nominal blade sectional chord (ft)
ε	tab extension length (% of nominal blade sectional chord)
η	tab deflection angle (deg)
C_l	sectional lift coefficient (normalized using extended airfoil chord)
C_d	sectional drag coefficient (normalized using extended airfoil chord)
C_m	sectional pitching moment coefficient (normalized using extended airfoil chord)
$C_{l_{eff}}$	sectional lift coefficient (normalized using nominal airfoil chord)
$C_{d_{eff}}$	sectional drag coefficient (normalized using nominal airfoil chord)
$C_{m_{eff}}$	sectional pitching moment coefficient (normalized using nominal airfoil chord)
α	sectional angle of attack (deg)
M	sectional mach number
ϕ	sectional elastic twist (deg)
$\vec{z}$	normalized 1/rev vibration vector
$\vec{u}$	tab control vector
F_x	hub longitudinal force (lbs)
F_y	hub lateral force (lbs)
F_z	hub vertical force (lbs)
J	total cost function
L_{hub}	hub roll moment (lbs)
M_{hub}	hub pitch moment (lbs)
S_x	blade root radial shear (lbs)
S_y	blade root chordwise shear (lbs)
S_z	blade root vertical shear (lbs)
M_x	blade root torsional moment (ft-lbs)
M_y	blade root flap bending moment (ft-lbs)
T	vibration sensitivity matrix with respect to control adjustments
V	Airspeed (knots)
$()_k$	pertaining to the k^{th} iteration
$()_z$	pertaining to vibratory loads
$()_u$	pertaining to control adjustments
$()_V$	pertaining to each airspeed
$()_{0P}$	pertaining to the steady component
$()_{1P}$	pertaining to the 1/rev component
$()_{2P}$	pertaining to the 2/rev component

Presented at the AHS Specialists' Conference on Aeromechanics Design for Transformative Vertical Flight, San Francisco, CA, January 16–19, 2018.

$()_{base}$ pertaining to the baseline case

INTRODUCTION

Blade-to-blade dissimilarities are prevalent in rotary-wing aircraft despite tight manufacturing tolerances. The unevenness between blades contributes to vibrations experienced in the fuselage, primarily at 1/rev (1P) but also at higher harmonics. Such a condition is commonly known as a rotor track-and-balance (RT&B) problem and can significantly increase crew and passenger fatigue, reduce component reliability, and shorten component life (Ref. 1). Historically, the solution to this problem involved passive adjustment of trim tabs on blades, pitch link lengths, and blade mass based on identified sensitivities to minimize vibration levels (Refs. 2–4). This process requires dedicated maintenance flights which are time-consuming, expensive, and necessitate adjustments to be made on ground. Since the adjustments also do not change with flight condition (e.g. cruise speed), the reductions in vibratory loads are sub-optimal across the flight envelope. The ability to change one or more of the adjustments in-flight allows for optimal settings at different flight conditions and can also compensate for progressive deterioration, which in turn would reduce the need for dedicated maintenance flights or eliminate them altogether. This approach falls under the umbrella of active track and balance.

Early efforts in this area focused on demonstrating feasibility of actuation mechanisms. Active trailing-edge tabs using shape-memory alloys (SMAs) (Refs. 5–7) and electromechanical actuators (Ref. 8) have been considered. However, only implementation aspects were evaluated and their effectiveness over passive trim tabs in reducing vibrations was not addressed. Recently, variable-length, low-bandwidth active pitch links were considered in Refs. 9–11 for in-flight tuning (IFT). In particular, Ref. 10 showed that the active pitch links *alone* were quite effective in minimizing vibration levels due to imbalance on a UH-60 rotor in the wind tunnel and were utilized successfully again on a CH-53G in flight tests (Ref. 11).

In recent years, there has been much interest in the area of rotor chord extension morphing (Refs. 12–17). Although the prior work cited has focused on its benefits in stall-dominant operating conditions, the actuation mechanism considered (an extendable trailing-edge plate) could also be exploited for in-flight rotor smoothing. As an alternative to the traditional *bendable* trailing-edge tab, an *extendable* trailing-edge tab over a spanwise portion of the blade can be deployed differentially from blade-to-blade, to minimize vibration due to blade dissimilarity. As with the active pitch links, the active trailing-edge tab settings can be changed with flight condition to achieve the maximum reductions in imbalance loads over the flight envelope and to compensate for progressive deterioration.

The present study compares the effectiveness of active pitch links and active trailing-edge tabs for in-flight rotor smoothing. A simulation model of the UH-60 rotor with seeded imbalance is developed and the resulting 1P vibratory loads are minimized using a weighted least-squares optimization method. The benefits of in-flight (active) tuning over conventional, on-ground (passive) adjustments for both mechanisms is assessed and sensitivity of the 1P vibratory loads over multiple flight regimes is also discussed in detail. Finally, the physics of both pitch link and trailing-edge tab is examined to understand the source of vibration reduction over the flight regime.

SIMULATION MODEL

A simulation model of the UH-60 Black Hawk rotor has been developed in the Rotorcraft Comprehensive Analysis System (RCAS) (Ref. 18). Key properties of the rotor blade are described in Table 1.

Table 1: UH-60 Rotor Properties

Rotor Radius	26.8 ft
Blade Chord	1.73 ft (mean)
Blade Twist	Nonlinear
Rotor Speed	258 RPM
Shaft Tilt	Scheduled with airspeed
Solidity	0.0822
Hinge Offset	1.25 ft
Blade Airfoil	SC1095 (root to 40% span) SC1094R8 (40-83% span) SC1095 (83% span to tip)

Main Rotor

The structural model of the UH-60 rotor is composed of a series of elements including rigid bars, linear rotational and translational springs and dampers, a rigid body mass, hinges, sliders and 13 nonlinear beam finite elements (Ref. 19). The outboard tip of the blade is swept and the blade is twisted nonlinearly along the radius. The pitch control linkage is represented by a series of rigid bars and spring elements and the collective and cyclic pitch inputs are introduced through a slide element. The blade root hinge is offset slightly from the center of rotation and the actual elastomeric bearing on the hub is represented by three discrete coincident hinge elements for flap, lag, and pitch rotation of the blade. The blades themselves are modeled as elastic beams undergoing coupled flap bending, lag bending, and elastic torsion. To introduce aerodynamic forces, the blade planform is discretized into 27 aerodynamic segments. Elemental aerodynamic forces and moments per unit length are calculated using airfoil look-up tables and distributed (via interpolation) across the blade.

The coupled aeroelastic response is calculated/applied in the locally deformed airfoil coordinates as the blade undergoes rigid and elastic deformations. Lastly, the rotor inflow is modeled using a 12 x 12 Peters-He finite-state dynamic inflow model (Ref. 20). Physical properties for all elements of the UH-60 rotor model were included as appropriate.

Pitch Links

Refs. 9 and 10 employ smart pitch rods to input small adjustments in blade pitch for track and balance on top of standard swashplate inputs. A similar method is employed in RCAS but through the use of an auxiliary pitch hinge on the blade. This hinge is co-located at the connection point of the pitch horn and the blade. It is designated as a controllable input in order to provide quasi-static adjustments to individual blade pitch for track-and-balance corrections.

Trailing-Edge Tabs

Instead of the traditional *bendable* trim tab, an alternative mechanism of an *extendable* trim tab is employed. This is accomplished through the use of an extendable trailing-edge plate (TEP) that has been used in prior studies as a method of chord-extension morphing (Ref. 13). The active, extendable tab mechanism is illustrated in Figure 2, taken from Ref. 13. As shown in the figure, the tab extension, ε, is given as a percent of the nominal airfoil chord and the angle of deflection, η, is measured relative to the baseline airfoil's chord line and is implemented between 63% and 83% of the blade span. The extension of the tab effectively alters the sectional aerodynamic coefficients through the extended chord length as well as the change in resulting airfoil profile. These modified coefficients are calculated using computational fluid dynamics (CFD) analysis and are detailed in Ref. 21. The baseline model of the UH-60A rotor uses coefficients from airfoil tables for both SC-1095 and SC-1094R8 which are normalized with respect to the *nominal* chord whereas the coefficients reported in Ref. 21 are normalized with respect to the *extended* chord. To maintain consistency of implementation, the sectional aerodynamic coefficients (C_l,C_d,C_m) in Ref. 21 are re-normalized with respect to the *nominal* chord of the baseline airfoil. The relation between these normalizations is as follows:

$$\begin{aligned} C_{l_{eff}} &= (1+\varepsilon)\, C_l \\ C_{d_{eff}} &= (1+\varepsilon)\, C_d \\ C_{m_{eff}} &= (1+\varepsilon)^2\, C_m \end{aligned} \tag{1}$$

Doing so provides effective values for lift ($C_{l_{eff}}$), drag ($C_{d_{eff}}$), and pitching moment ($C_{m_{eff}}$) coefficients as a function of the *nominal* chord and also allows for ease of implementation in RCAS, where the tab is modeled as an aerodynamic flap segment. Lastly, the effective aerodynamic coefficients are tabulated into look-up tables as a function of angle of attack α, mach number M, and tab extension ε. Figure 1 shows these aerodynamic coefficients for the baseline SC-1094R8 airfoil and the modified variants that incorporate a maximum tab extension of $\varepsilon = 20\%$ and deflection angles of $\eta = 0°, 2°, 4°$, at a mach number of $M = 0.4$.

Imbalance Loads

Rotor smoothing on the UH-60 is typically conducted on the ground, in hover, and at 80 knots, 120 knots, and 145 knots cruise (Refs. 3, 4). In Ref. 10, vibratory loads due to dissimilarity are reported for rotor advance ratios of $\mu = 0.2$ (90 knots) and $\mu = 0.35$ (155 knots) for the UH-60 rotor. To create a baseline vibration profile, these loads are then extrapolated to include hover, 80, 120, and 145 knots as well. For implementation in RCAS, mechanical point loads are applied with a specific magnitude and phase at the root of one blade such that appropriate vibration levels are generated at the hub for each airspeed.

Trim

A wind-tunnel trim procedure is carried out in RCAS for the UH-60A rotor. The rotor collective (θ_0), lateral (θ_{1c}), and longitudinal (θ_{1s}) cyclic pitch are used to trim the hub vertical force to 15,250 lbs and hub roll and pitch moments to 0 ft-lbs. The longitudinal shaft tilt angle (α_s) is set at prescribed values scheduled with airspeed, shown in Table 2. To trim the rotor at a given flight condition, an azimuthal step of 5° is used to calculate the aerodynamic loads on the blade and find a converged periodic solution for integrated rotor loads, inflow, and blade deformations over several revolutions. The three trim variables are then perturbed to determine the Jacobian matrix and trim steps are taken iteratively until the residuals of vertical force and roll/pitch moments are within specified tolerances.

Table 2: Rotor Longitudinal Shaft Tilt

V (knots)	α_s (deg)
0	0
80	−1.42
120	−4.5
145	−7

MINIMIZATION OF VIBRATORY LOADS

To minimize the vibratory loads resulting from rotor imbalance, a weighted least-squares optimization method

is employed. Specifically, the 1/rev (1P) hub loads are targeted by the optimizer. The hub vibration levels can be written as a linearized equation in the following form:

$$\vec{z}_{k+1} = \vec{z}_k + T\Delta\vec{u}_k \tag{2}$$

$\vec{z}_k$ represents the vector of normalized 1P vibration magnitudes and $\vec{u}_k$ represents the vector of tab or pitch link controls on each blade, respectively, for the k^{th} iteration in the optimization process:

$$\vec{z}_k = \begin{bmatrix} F_{x_{1P}}/F_{x_{1P_{base}}} \\ F_{y_{1P}}/F_{y_{1P_{base}}} \\ F_{z_{1P}}/F_{z_{1P_{base}}} \\ M_{x_{1P}}/M_{x_{1P_{base}}} \\ M_{y_{1P}}/M_{y_{1P_{base}}} \end{bmatrix}_k , \ \vec{u}_k = \begin{bmatrix} \varepsilon_1 \\ \varepsilon_2 \\ \varepsilon_3 \\ \varepsilon_4 \end{bmatrix}_k \quad or \quad \vec{u}_k = \begin{bmatrix} \theta_1 \\ \theta_2 \\ \theta_3 \\ \theta_4 \end{bmatrix}_k \tag{3}$$

where $F_{x_{1P_{base}}}$, $F_{y_{1P_{base}}}$, $F_{z_{1P_{base}}}$, $M_{x_{1P_{base}}}$, and $M_{y_{1P_{base}}}$ are the baseline (uncontrolled) vibration levels. The variable T in Equation 2 is a sensitivity matrix, whose columns are obtained from the change in vector $\vec{z}_k$ by perturbing the elements of the vector $\vec{u}_k$, i.e. the Jacobian of the vibratory loads with respect to the controls. Both the calculation of 1P loads and the T-matrix are carried out in RCAS as part of the optimization process. The scalar cost function for the optimization is written as

$$J = J_z + J_u = \vec{z}_{k+1}{}^T W_z \vec{z}_{k+1} + \vec{u}_k{}^T W_u \vec{u}_k \tag{4}$$

In Equation 3, J is a cost function that represents the sum of the weighted squares of the vibration measurements (J_z) and the control adjustments (J_u). W_z and W_u correspond to the weights pertaining to the vibratory loads and control adjustments, respectively. In this study, both weighting matrices are set as identities

$$W_z = \mathcal{I}_{5x5} \ , \ W_u = \mathcal{I}_{4x4} \tag{5}$$

A schematic of the optimization process is shown in Figure 3.

Passive Track-and-Balance

For conventional passive track-and-balance procedures (with no in-flight adjustments), the $\vec{u}$ settings represent a compromise over the flight-speed regime. Thus, the optimization problem would be framed as

$$\begin{aligned} Determine \quad \vec{u} = \begin{bmatrix} \varepsilon_1 \\ \varepsilon_2 \\ \varepsilon_3 \\ \varepsilon_4 \end{bmatrix} \quad or \quad \vec{u} = \begin{bmatrix} \theta_1 \\ \theta_2 \\ \theta_3 \\ \theta_4 \end{bmatrix} \quad to \qquad (6) \\ minimize \quad J_{comp} = J_z + J_u = W_{z_0} J_{z_0} + W_{z_{80}} J_{z_{80}} + W_{z_{120}} J_{z_{120}} \\ + W_{z_{145}} J_{z_{145}} + W_u J_u \\ subject \quad to \quad 0\% \leq \vec{u} \leq 20\% \end{aligned}$$

The cost function pertaining to the vibration measurements (J_z) is now a sum of loads at multiple airspeeds. W_{z_0}, $W_{z_{80}}$, $W_{z_{120}}$, $W_{z_{145}}$ and J_{z_0}, $J_{z_{80}}$, $J_{z_{120}}$, $J_{z_{145}}$ correspond to the weights and cost functions pertaining to the vibratory loads, respectively, at those airspeeds. Note that a total of four tab/pitch link settings are available in all, to minimize vibration levels over all flight speeds.

Active Track-and-Balance

Consider next, the case where the tab or pitch link settings are active. The optimization problem is now solved separately at each airspeed, V, and framed as

$$\begin{aligned} Determine \quad \vec{u}_V = \begin{bmatrix} \varepsilon_1 \\ \varepsilon_2 \\ \varepsilon_3 \\ \varepsilon_4 \end{bmatrix}_V \quad or \quad \vec{u}_V = \begin{bmatrix} \theta_1 \\ \theta_2 \\ \theta_3 \\ \theta_4 \end{bmatrix}_V \quad to \qquad (7) \\ minimize \quad J_V = J_{z_V} + J_{u_V} \\ subject \quad to \quad 0\% \leq \vec{u}_V \leq 20\% \end{aligned}$$

with J_{z_V} and J_{u_V} defined similar to Equation 4. The solutions would then take the form

$$\vec{u}_0 = \begin{bmatrix} \varepsilon_1 \\ \varepsilon_2 \\ \varepsilon_3 \\ \varepsilon_4 \end{bmatrix}_0 \quad \vec{u}_{80} = \begin{bmatrix} \varepsilon_1 \\ \varepsilon_2 \\ \varepsilon_3 \\ \varepsilon_4 \end{bmatrix}_{80} \quad \vec{u}_{120} = \begin{bmatrix} \varepsilon_1 \\ \varepsilon_2 \\ \varepsilon_3 \\ \varepsilon_4 \end{bmatrix}_{120} \quad \vec{u}_{145} = \begin{bmatrix} \varepsilon_1 \\ \varepsilon_2 \\ \varepsilon_3 \\ \varepsilon_4 \end{bmatrix}_{145} \tag{8}$$

$$\vec{u}_0 = \begin{bmatrix} \theta_1 \\ \theta_2 \\ \theta_3 \\ \theta_4 \end{bmatrix}_0 \quad \vec{u}_{80} = \begin{bmatrix} \theta_1 \\ \theta_2 \\ \theta_3 \\ \theta_4 \end{bmatrix}_{80} \quad \vec{u}_{120} = \begin{bmatrix} \theta_1 \\ \theta_2 \\ \theta_3 \\ \theta_4 \end{bmatrix}_{120} \quad \vec{u}_{145} = \begin{bmatrix} \theta_1 \\ \theta_2 \\ \theta_3 \\ \theta_4 \end{bmatrix}_{145}$$

Unlike the passive track-and-balance case, four tab settings are now available at *each* speed.

VALIDATION

Before minimizing 1P vibration levels over the flight envelope, the implementation of active pitch links in RCAS was validated against wind-tunnel results reported in Ref. 10. The flight conditions, initial vibration levels, and optimization routine was configured in RCAS to match the wind-tunnel setup as closely as possible. In particular, the optimizer was setup to minimize only the 1P lateral force and pitching moment using pitch offsets on blades 1 and 2 alone. Figure 4 shows validation results for an advance ratio of $\mu = 0.2$. As seen in Figure 4a, the reduction in lateral force correlates well with in-flight tuning (IFT) results (Ref. 10). On the other hand, RCAS predicts smaller reductions in pitching moment compared to test data. This difference could in part be attributed to possible discrepancies in trim controls between the model and experiment. Figure 4b shows a

comparison of the pitch link controls from RCAS with IFT results. While the magnitudes show some difference, the overall trend of control adjustment is captured reasonably well in the present simulation.

RESULTS AND DISCUSSION

As mentioned earlier, representative 1P vibratory loads were seeded on the UH-60 rotor model and subsequently minimized over a range of airspeeds. Note that all results described in this paper pertaining to the trailing-edge tabs are for a deflection angle of $\eta = 2°$. Additionally, as part of the optimization procedure for both passive and active cases, multiple initial guesses for the control vector, $\vec{u}$, were tested in an effort to capture the best possible optimum at all airspeeds. Initial values of 0%, 10%, and 20% were used for tab extension and -0.66^o, 0^o, 0.66^o were used for the pitch link.

Minimization of 1P Loads

Figures 5a-5c show 1P hub lateral force, vertical force, and pitching moment loads using trailing-edge tab controls. Both passive adjustments (that do not change over the airspeed regime), as well as active adjustments (determined at 0, 80, 120 and 145 knots) are considered and the respective tab controls are shown in Figure 5d. Figures 6a-6d show a similar set of results using pitch link controls.

Trailing-Edge Tabs In hover, the passive tab shows a large reduction in 1P lateral force (Figure 5a), with the active tab showing further reduction (87% compared to 68%). At 80, 120 and 145 knots, both active and passive adjustments show comparable reductions in 1P lateral hub forces. Relative to hover, the reductions are seen to be modest at intermediate cruise speeds (80 and 120 knots), before increasing again somewhat in high-speed cruise (145 knots), but not to the levels of reduction observed in hover. 1P vertical force does not show any reduction in hover but progressively larger reductions are observed at increasing forward flight speeds (Figure 5b). Over the 80-145 knots flight speed range, active tab adjustments show significantly larger reductions in 1P vertical loads (87%) as compared to adjustments with the passive tab (46%). Modest reductions in 1P hub pitching moments (Figure 5c) are observed over the entire airspeed range with active tab adjustments showing only a small improvement (34%) in hover over the passive adjustments (24%). Figure 5d shows the required tab settings calculated from the optimization process. Clearly, the controls required to achieve the minimum vibration levels vary significantly with flight condition, which is only realizable with an active mechanism.

Pitch Links The passive pitch link shows a large reduction for 1P lateral force in hover (Figure 6a), with the active case showing further reduction (85% compared to 66%). At the remaining cruise speeds, both active and passive pitch link adjustments show similar reductions in 1P lateral hub forces, which was also observed with the tab. However, the magnitude of the reductions are much larger using the pitch link mechanism (80%), as shown by comparison of Figures 5a and 6a. For 1P vertical force, no reduction is seen in hover but the trend is similar to that of Figure 5b with increasing forward flight speeds. Note, however, that both passive and active cases of the pitch link mechanism show similar levels of reduction. Comparing Figures 5b and 6b, the active tab shows slightly higher reductions in 1P vertical force over the active pitch link. However, comparing Figures 5a and 5b to 6a and 6b, the active pitch link is much more effective at simultaneously reducing both 1P lateral force and 1P vertical force, which is not observed with the active tab. The reductions in 1P pitching moment are observed to be relatively moderate throughout the flight regime, similar to Figure 5c, with the active and passive pitch link adjustments again showing similar results. Comparing Figures 5c and 6c shows that using the pitch link over the extendable tab produces a slightly lower vibration profile in cruise while showing comparable values in hover. Figure 6d shows the required pitch link settings over the airspeed range. Unlike the trailing-edge tab, the controls required do not change significantly with flight condition, which favors usage as a passive mechanism.

Sensitivity Analysis

The sensitivity of the 1P lateral forces to trailing-edge tab and pitch link controls across flight speeds is shown in Figures 7 and 8, respectively. For each polar plot in these figures, the black dot indicates the magnitude and phase of the uncontrolled vibration levels. In Figure 7, the tab on each blade is deployed *individually* from 0-20% and the corresponding change in 1P vibration level is indicated by the line associated with the specific blade. Similarly, in Figure 8, the pitch link setting on each blade is reduced *individually* from 0^o to -1^o and the changes in 1P vibration levels are recorded. As seen in Figure 7, the lateral force displays modest sensitivity to tab deployment at hover but sensitivity reduces significantly at 80 and 120 knots before increasing again at 145 knots (but not to the degree observed in hover). In the case of pitch link adjustments (Figure 8), the lateral force displays significantly more sensitivity in hover and retains effectiveness at 80 and 120 knots compared to the trailing-edge tab, before again rising to near-hover levels at 145 knots. The trends shown across airspeeds in Figures 7 and 8 are observed to be consistent with the vibration results shown in Figures 5a and 6a.

Figures 9 and 10 show the sensitivity of the 1P vertical force to tab and pitch link controls, respectively. Zero sensitivity is observed for vertical force in hover since quasi-static tab or pitch link adjustments cannot gener-

ate any counteracting 1P vertical loads. In forward flight, however, the presence of cyclic pitch and azimuthal variation in incident velocity allow the generation of counteracting 1P vertical loads. From 80 to 145 knots, both tab and pitch link controls consistently show strong sensitivity in 1P vertical force, with the pitch link showing slightly higher sensitivity compared to the tab. Similarly, over all airspeeds, both tab and pitch link controls show moderate sensitivity for 1P pitching moment, as seen in Figures 11 and 12. The pitch link sensitivities, however, are slightly larger compared to the tab. As with the lateral force, the sensitivity trends of vertical force and pitching moment are consistent with the results shown in Figures 5b, 5c, 6b, and 6c, respectively.

It is interesting to note that the polar sensitivity plots for the tab (Figures 5a, 5b, 5c) all indicate that deployment of the tab on blade 2 would be most effective in reducing vibration. This is consistent with the optimized tab deflection results in Figure 5d. In Figures 9b-9d, the sensitivity of 1P vertical vibration levels in cruise to blade 2 tab deployment seems to be so strong that deploying this tab to its maximum (20%) to reduce lateral force or pitching moment could result in over-actuating the system for 1P vertical force. It is not surprising, then, that at 80 to 145 knots, the optimizer does not allow the tab on blade 2 to deflect to its maximum (Figure 5d) and appears to compensate, in part, with blade 4 tab deflection. Similarly, the polar sensitivity plots for the pitch link (Figures 8, 10, 12) indicate that reduction of pitch on blade 2 would be most effective in reducing vibration. Figure 12 dictates that a full -1^o pitch change on blade 2 is required to maximize reduction in 1P pitching moments. However, doing so incurs a significant penalty in *both* 1P lateral and vertical force, as opposed to the tab where the penalty was primarily incurred in the vertical force *alone*.

Physics of Vibration Reduction

To understand the method by which the vibratory loads are reduced, the underlying physics of both tab and pitch link mechanisms are now explored in further detail. Specifically the analysis considers the blade root shears and moments that contribute to the 1P vibratory loads at the hub. Table 3 summarizes the contributing components to the 1P loads at the hub, where S_x, S_y, and S_z are radial, chord-wise, and vertical blade root shears and M_x and M_y are blade root torsional and flap-bending moments, respectively. The coordinate system used for the root shears and moments is defined as follows: S_z is defined positive upwards, S_x is defined positive radially outward (towards blade tip), and S_y is defined positive in the direction of blade lead. For the moments, M_x is defined positive nose-up while M_y is positive for blade flapping downward.

Table 3: Transmission of Blade Root Shears to 1P Hub Loads

Hub 1P Loads		Blade Root Shears
$F_{z_{1p}}$	from	$S_{z_{1p}}$
$F_{x_{1p}}, F_{y_{1p}}$	from	$S_{x_{0p}}, S_{y_{0p}}, S_{x_{2p}}, S_{y_{2p}}$
L_{1p}, M_{1p}	from	$M_{x_{0p}}, M_{y_{0p}}, M_{x_{2p}}, M_{y_{2p}}$

Hover The axisymmetric flow condition in hover facilitates ease of analysis and serves as a good starting point for understanding the operational mechanisms by which 1P vibration reduction is achieved. From Figures 1a-1c, at $\eta = 2^o$, it is seen that the extension of the tab generally increases sectional lift, drag, and nose-down pitching moment. For the relatively torsionally compliant UH-60 rotor, a nose-down pitching moment induces a significant nose-down elastic twist. Figure 13a shows the change in twist on each blade corresponding to the active tab hover inputs from Figure 5d. The large tab deflections on blades 2 and 4 are clearly observed to produce a nose-down elastic twist (relative to blades 1 and 3). Figure 13b shows the corresponding change in chord-wise shear force on each blade. On both Figures 13a and 13b, the dashed-dotted black vertical lines correspond to the 63% to 83% region over which the tab is present. While the drag on blade 2 generally decreases along the span due to nose-down twist (resulting in a net positive ΔS_y), the local effect of the drag due to tab extension is clearly visible on Figure 13b. In summary, a large change in chordwise force is generated on blade 2 (pointing toward the leading edge) and a smaller change in chordwise force is generated on blade 4 (also pointing to the leading edge) due to tab deflection on the two blades. Similarly, in the case of the pitch link, differences in the change in chordwise force between blades 2 and 4 are generated through adjustment of the root pitch of the respective blades, as shown in Figure 14.

Figure 15 pictorially depicts the mechanism of vibration reduction through the trailing-edge tab. The seeded imbalance in radial shear on blade 1 is counteracted by the change in steady chordwise shear ($\Delta S_{y_{0p}}$) generated on blades 2 and 4. Similarly, the seeded imbalance in torsion moment on blade 1 is counteracted by the change in steady flapwise bending moment ($\Delta M_{y_{0p}}$) on blades 2 and 4. The change in flapwise bending moment is primarily attributed to the change in lift on the blades due to the nose-down elastic twist seen in Figure 13a. A similar process is seen for the pitch link mechanism in Figure 16.

120 knots The process by which 1P hub lateral and pitching moment vibrations are reduced remains broadly the same as in hover for both tab and pitch link. However, at 120 knots, tab extensions are commanded on all four blades, as opposed to only blades 2 and 4 in hover (Figure 5d). In addition to change in chord-wise shear

on blades 2 and 4, changes in radial shear on blades 1 and 3 also contribute to the reduction in total 1P lateral hub vibrations (Figure 17). Similarly, in addition to change in flapwise bending moments on blades 2 and 4, a changes in torsional moments on blades and 1 and 3 also contribute to the reduction in total 1P hub pitching moment vibrations. In contrast, the process for the pitch link (Figure 18), only utilizes changes in chord-wise shear and flapwise bending moments on blades 2 and 4.

Trim Controls

Upon adjustment of the controls for rotor track-and-balance, it would be expected that the steady rotor forces and moments would go out of balance. Consequently, as part of the optimization process, the rotor is re-trimmed at every iteration of the optimization routine, as shown in Figure 3. Extending the trailing-edge tab is expected to locally increase the lift on the blade and necessitate a drop in rotor collective pitch to maintain thrust. However, Figure 19a shows little deviation in collective pitch from the uncontrolled case for both passive and active optimization methods. This is primarily due to the generation of nose-down elastic twist that counteracts the additional lift from the change in airfoil profile and larger blade chord, which results in practically zero change in required rotor collective pitch.

For pitch link adjustment, the rotor collective pitch (Figure 19b) reduces by the average values of the pitch link adjustments given in Figure 6d, as would be expected. It was verified that subtracting this average value from the controls given in Figure 6d results in the same vibration profile shown in Figures 6a-6c, which indicates that the differences in pitch between the blades is the primary method of vibration reduction whereas a uniform pitch change merely represents an offset point. The trim rotor cyclic pitch controls (θ_{1c} and θ_{1s}) for both tab and pitch link usage showed little change across airspeeds and are therefore not shown.

CONCLUSIONS

The current study focuses on the effectiveness of an active pitch link and an active trailing-edge tab mechanism in reducing rotor 1/rev (1P) loads due to blade dissimilarity. The pitch link mechanism produces a quasi-static adjustment of blade root pitch in addition to the inputs from the swashplate (Ref. 10). The tab mechanism is essentially an extendable trailing-edge-plate over a spanwise section of each blade similar to (Ref. 13). A simulation model of the UH-60 rotor is developed in RCAS and imbalance loads are seeded on one blade to simulate dissimilarity. The resulting 1P vibratory loads are then minimized using a weighted least-squares optimization method. Both active and passive adjustments of the two mechanisms are considered and a comparative analysis of the vibration profiles with pitch link and tab controls is undertaken. Sensitivities of the 1P vibratory loads to pitch link and tab controls are examined across the range of airspeeds. Lastly, the physics of both mechanisms is explored in hover and forward flight to understand the source of reduction in vibration. From the results presented in the paper, the following observations were drawn:

1. The extendable trailing-edge tab, as a mechanism, has the ability to reduce 1P imbalance loads. Its greatest effectiveness is in reducing the 1P in-plane forces in hover, and the 1P vertical forces in cruise. In cruise, the 1P in-plane forces show moderate reductions, with these reductions increasing again at high speed. The extendable tab is unable to reduce the 1P vertical shear in hover but shows the ability to introduce moderate reductions in 1P in-plane moments over the entire range of airspeeds.

2. Using an active extendable tab, instead of a passive tab, results in additional reductions in 1P in-plane forces in hover (reductions of 87% compared to 68% with the passive tab). The active extendable tab also results in additional decrease in 1P vertical force in cruise. At 80 knots, the active tab generates reductions of 87% compared to reductions of 46% with the passive tab. For the 1P in-plane moments, the active tab shows slight improvement over the passive tab (reductions of 34% compared to 24%) in hover. Best reductions in 1P vibration are achieved by varying the active tab inputs over the range of airspeeds. For seeded imbalance loads on blade 1, the optimizer yields active tab inputs for only blades 2 and 4 in hover and high-speed (145 knots), while tab extensions on all four blades are commanded at 80 and 120 knots. The passive tab extensions from the optimization results were observed to be lower than those of the active tab.

3. The pitch link shows a significant ability to reduce 1P lateral force over the entire range of airspeeds and simultaneously reduce vertical forces in cruise. Compared to the trailing-edge tab the reductions in 1P lateral forces in cruise are substantially larger. Reductions in 1P in-plane moments show a slight improvement over the trailing-edge tabs in cruise. However, using an active pitch link does not yield any appreciable benefits over a passive pitch link, with the exception of 1P lateral force in hover (reductions of 85% compared to 66%).

4. In hover, an examination of the imbalance load reduction process showed that generation of blade root chordwise shear on orthogonal blades (2 and 4 in the simulations carried out in this study) through the extension of the tab cancelled the seeded radial shear imbalance (on blade 1). The generation of blade root flap bending moments on orthogonal blades (2

and 4) through tab extension negated the seeded blade root torsion moment imbalance (on blade 1). A similar process is observed with the pitch link. At 120 knots, the underlying process remains similar for both tab and pitch link. However, changes in radial shear and torsion moment on blades 1 and 3 were also determined to be contributors to the total reductions in 1P hub lateral and pitching moment vibrations for the trailing-edge tab.

5. The required rotor collective pitch shows little change with trailing-edge tab extension primarily due to nose-down elastic twist which counteracts the additional lift from the change in airfoil profile and larger blade chord. For the pitch link, the rotor collective reduces by the average value of the adjustments across all blades. Subtracting this average value from the controls results in similar vibration profiles, which indicates that differences in blade pitch primarily drive vibration reduction whereas a uniform pitch change merely represents an offset point.

Author contact: Jayanth Krishnamurthi, krishj@rpi.edu; Farhan Gandhi, gandhf@rpi.edu

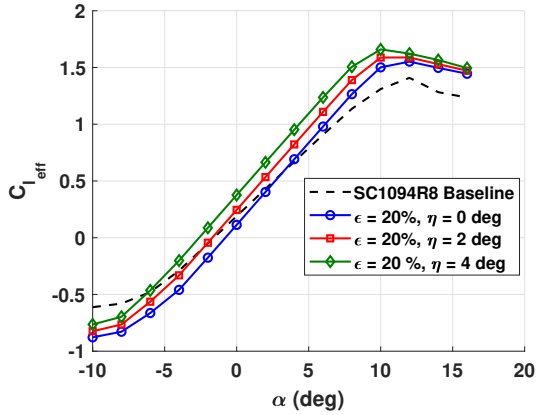

(a) Lift Coefficient

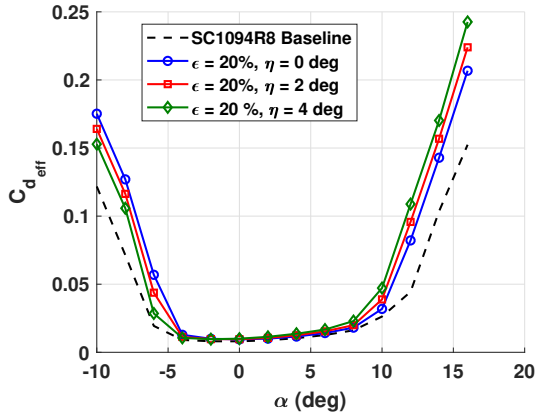

(b) Drag Coefficient

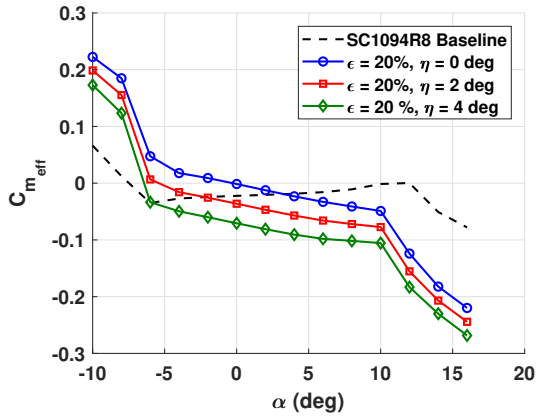

(c) Moment Coefficient

Fig. 1: Aerodynamic coefficients for baseline and extendable TEP for $M = 0.4$, normalized with respect to nominal chord, Ref. 21

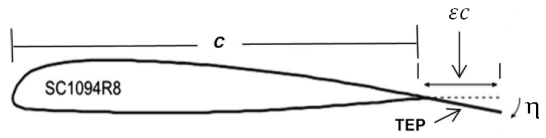

(a) TEP Extension - Airfoil

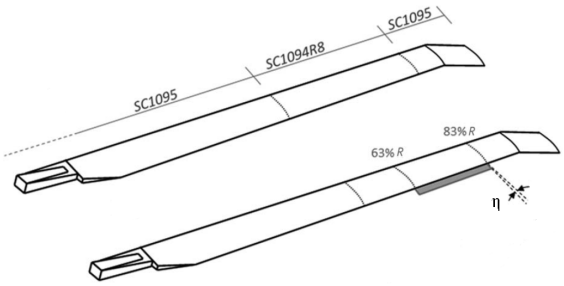

(b) TEP Extension - Blade

Fig. 2: Chord Extension Mechanism, Ref. 13

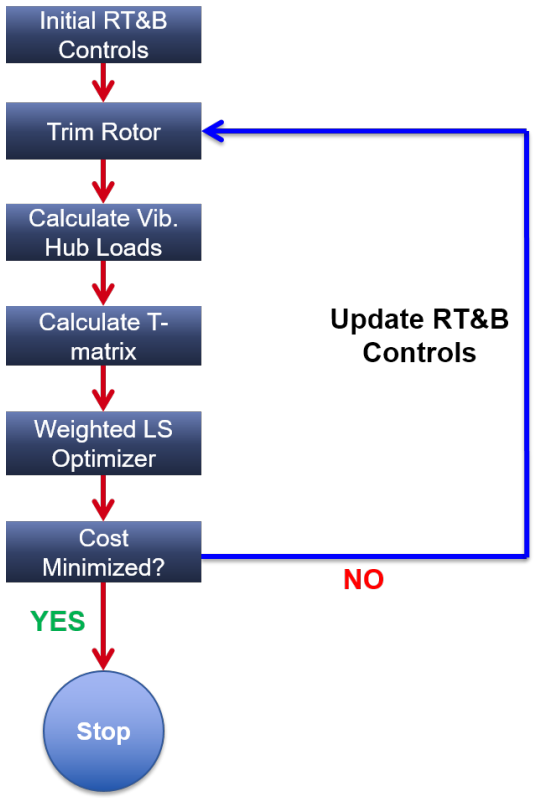

Fig. 3: Optimization Algorithm for Minimizing Vibratory Loads

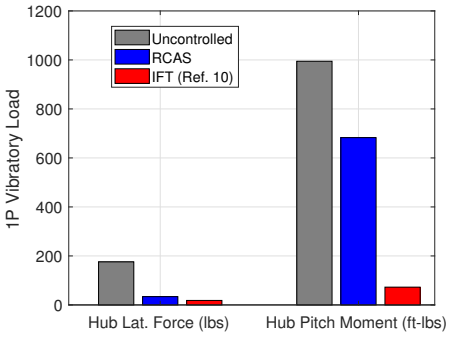

(a) 1P Lateral Force and Pitching Moment

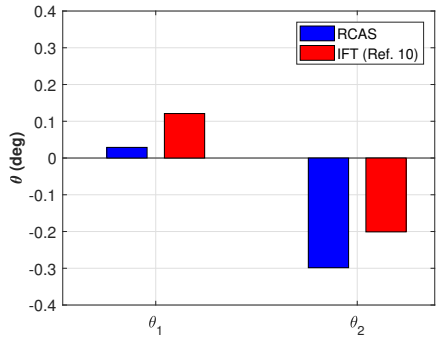

(b) Pitch Link Controls

Fig. 4: Active Pitch Link - Validation of Vibratory Loads and Controls, $\mu = 0.2$

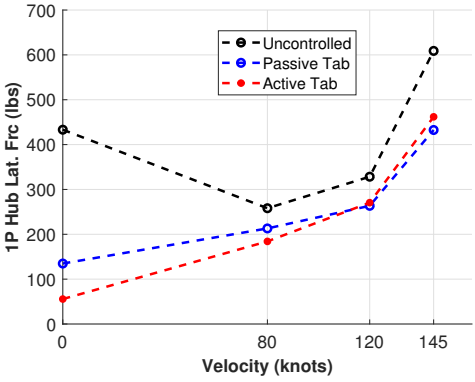

(a) 1P Lateral Force - Tab

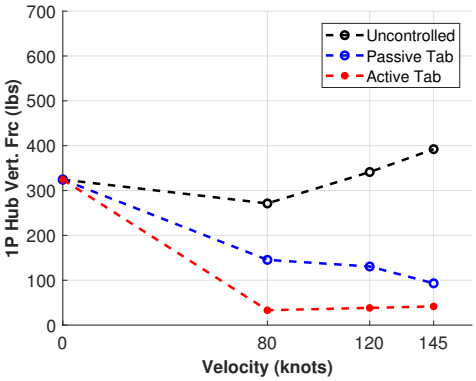

(b) 1P Vertical Force - Tab

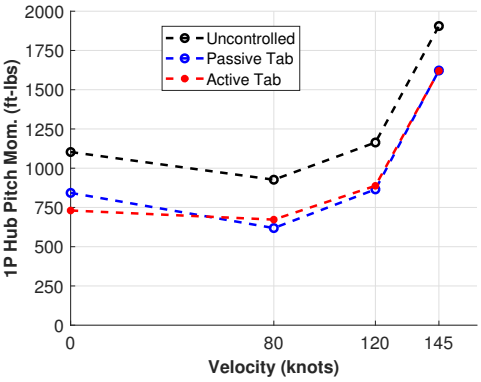

(c) 1P Pitching Moment - Tab

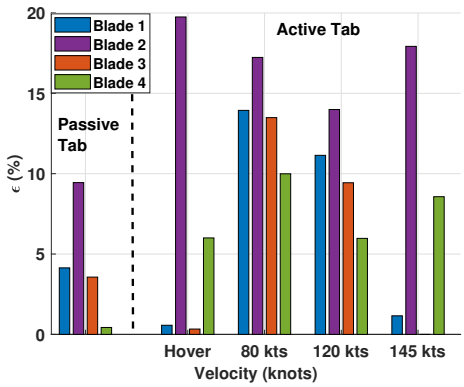

(d) Tab Controls

Fig. 5: Trailing-Edge Tab - 1P Vibration Levels and Controls

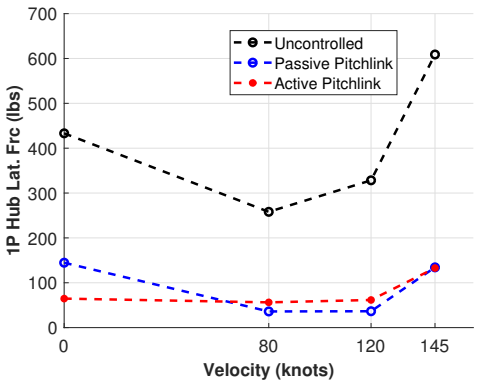

(a) 1P Lateral Force - Pitch link

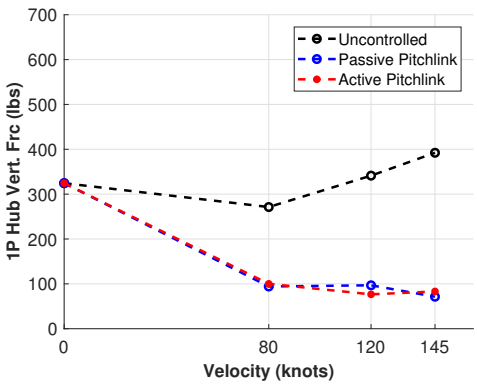

(b) 1P Vertical Force - Pitch link

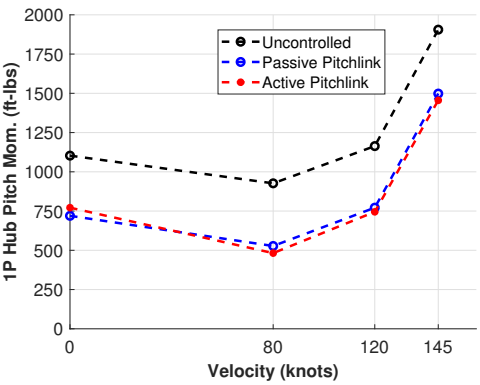

(c) 1P Pitching Moment - Pitch link

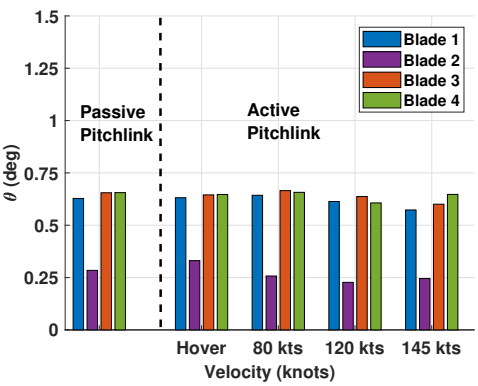

(d) Pitch link Controls

Fig. 6: Pitch link - 1P Vibration Levels and Controls

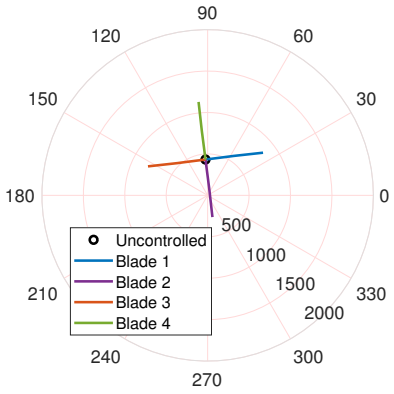

(a) Hover

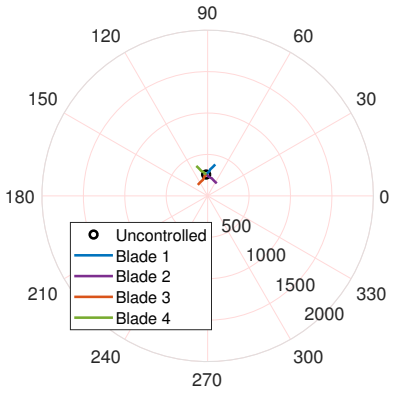

(b) 80 knots

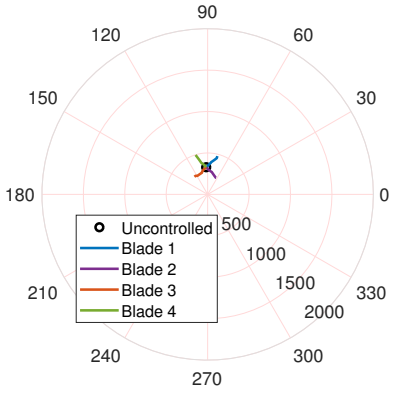

(c) 120 knots

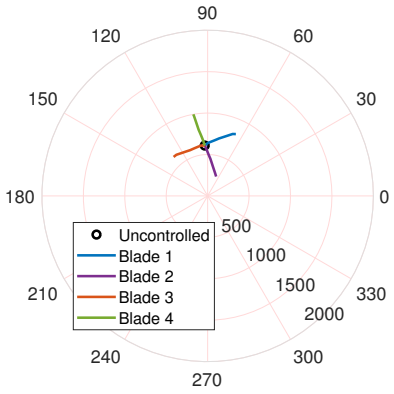

(d) 145 knots

Fig. 7: 1P Lat. Force Sensitivity to Trailing-Edge Tab

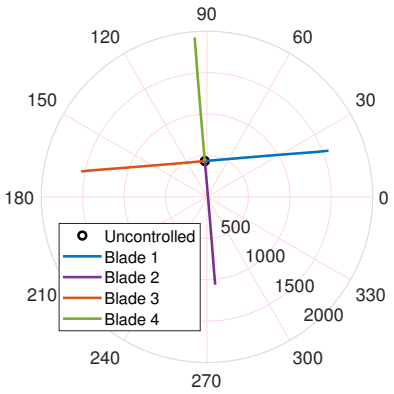

(a) Hover

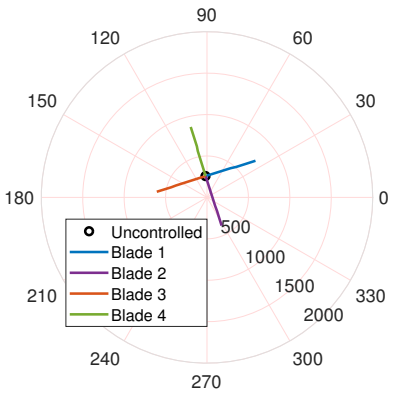

(b) 80 knots

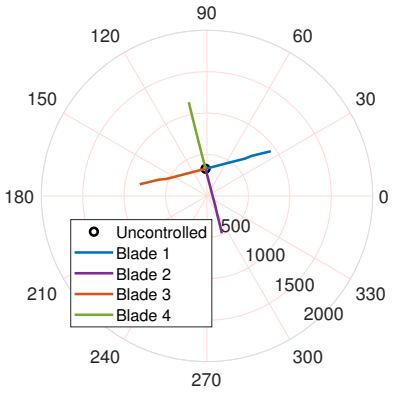

(c) 120 knots

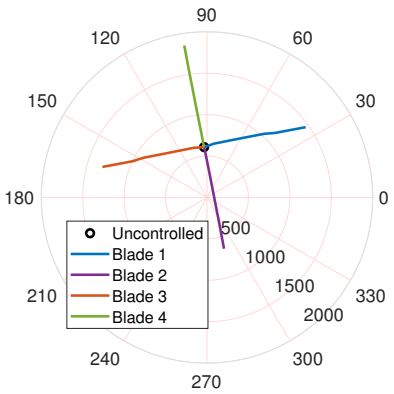

(d) 145 knots

Fig. 8: 1P Lat. Force Sensitivity to Pitch link

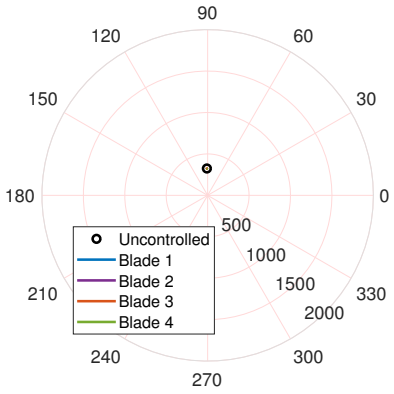

(a) Hover

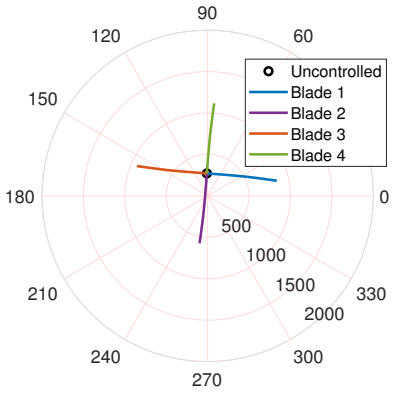

(b) 80 knots

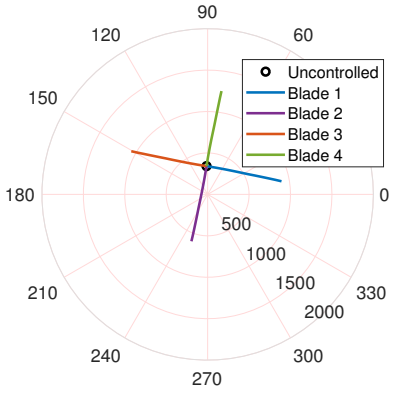

(c) 120 knots

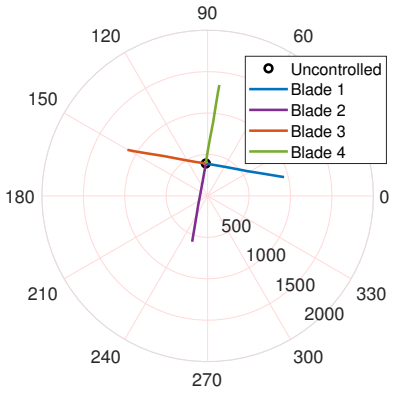

(d) 145 knots

Fig. 9: 1P Vert. Force Sensitivity to Trailing-Edge Tab

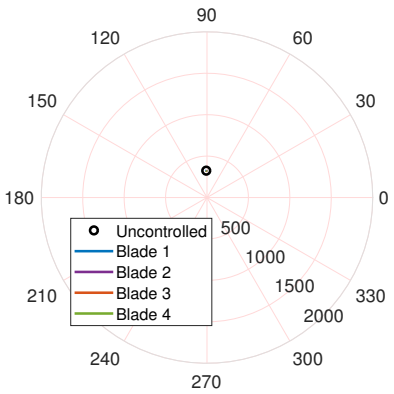

(a) Hover

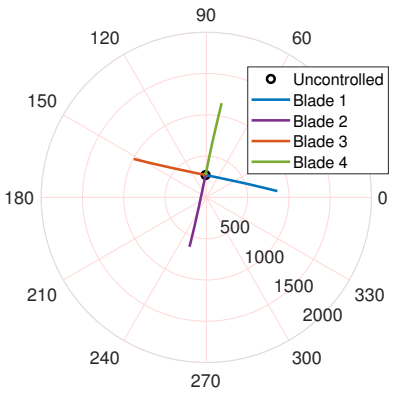

(b) 80 knots

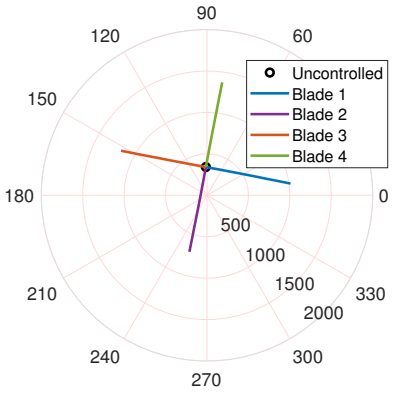

(c) 120 knots

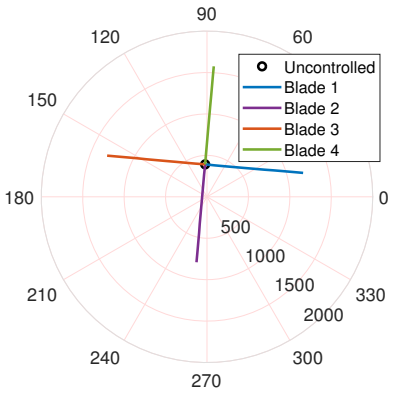

(d) 145 knots

Fig. 10: 1P Vert. Force Sensitivity to Pitch link

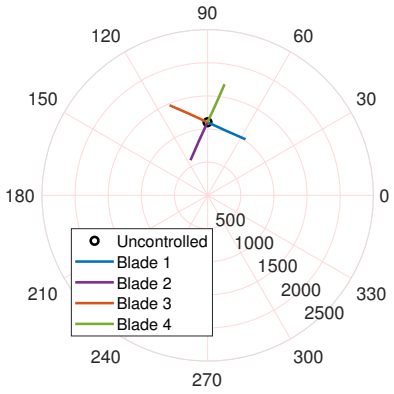

(a) Hover

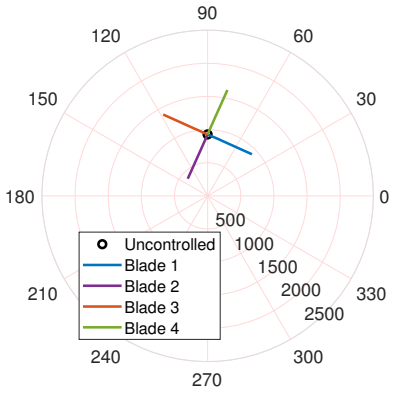

(b) 80 knots

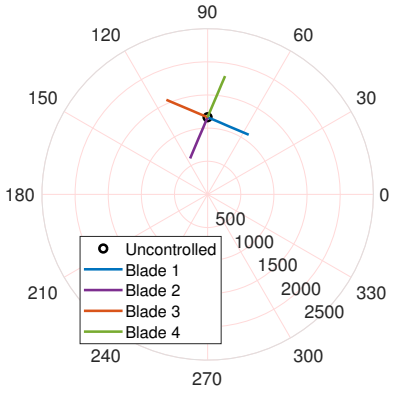

(c) 120 knots

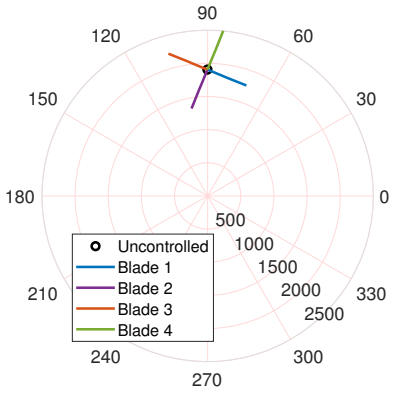

(d) 145 knots

Fig. 11: 1P Pit. Mom. Sensitivity to Trailing-Edge Tab

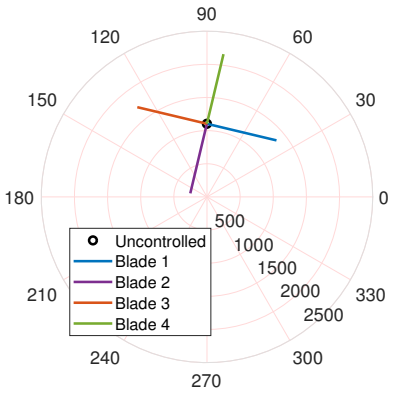

(a) Hover

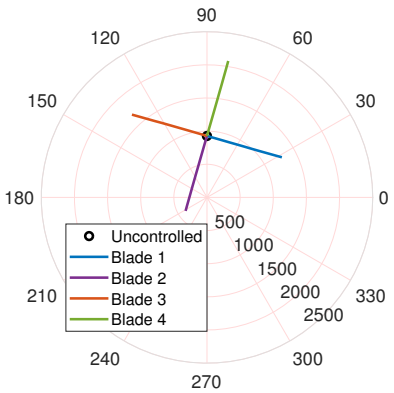

(b) 80 knots

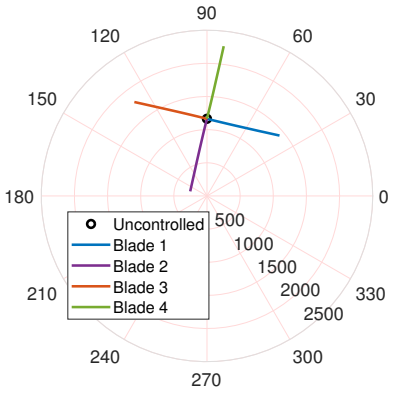

(c) 120 knots

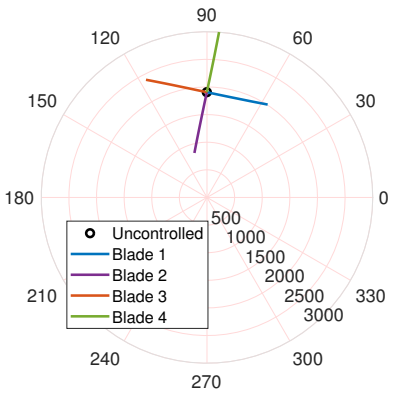

(d) 145 knots

Fig. 12: 1P Pit. Mom. Sensitivity to Pitch link

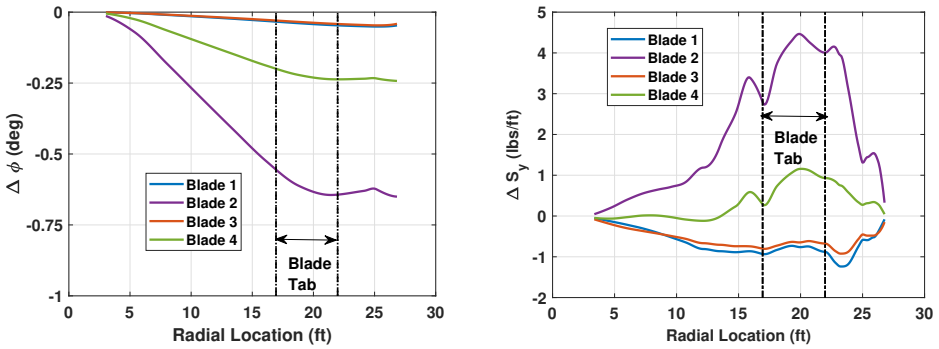

(a) Elastic Twist (b) Chord-wise Shear

Fig. 13: Trailing-Edge Tab - Elastic Twist and Chord-wise Shear in Hover

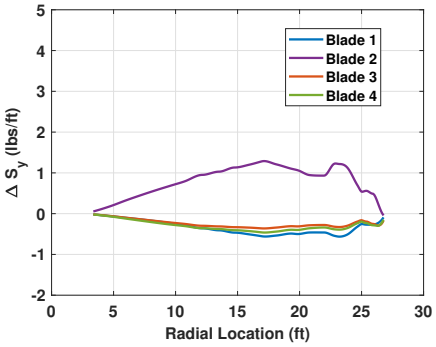

Fig. 14: Pitch link - Chord-wise Shear in Hover

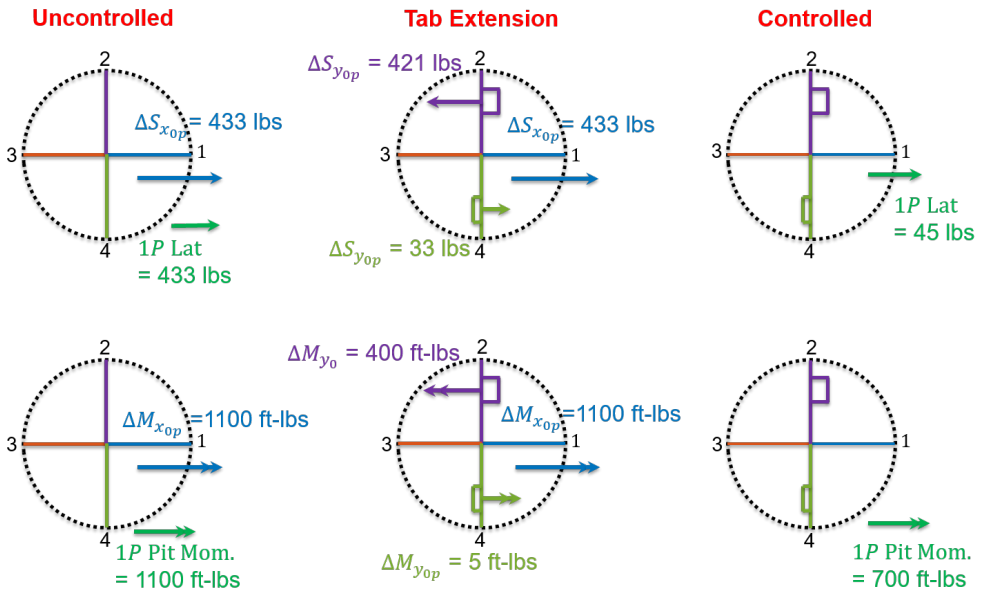

Fig. 15: Trailing-Edge Tab in Hover

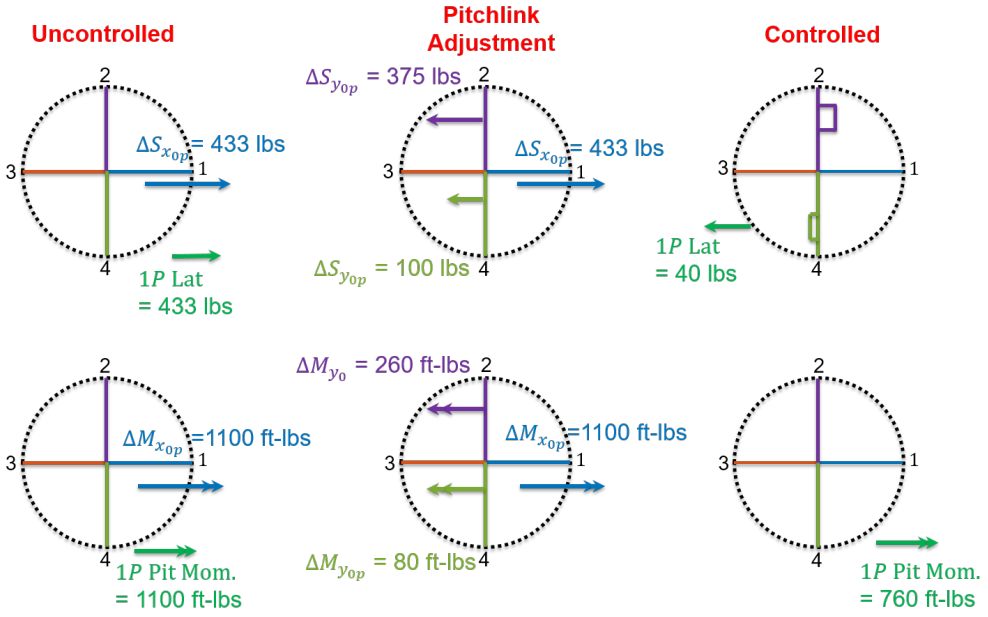

Fig. 16: Pitch link in Hover

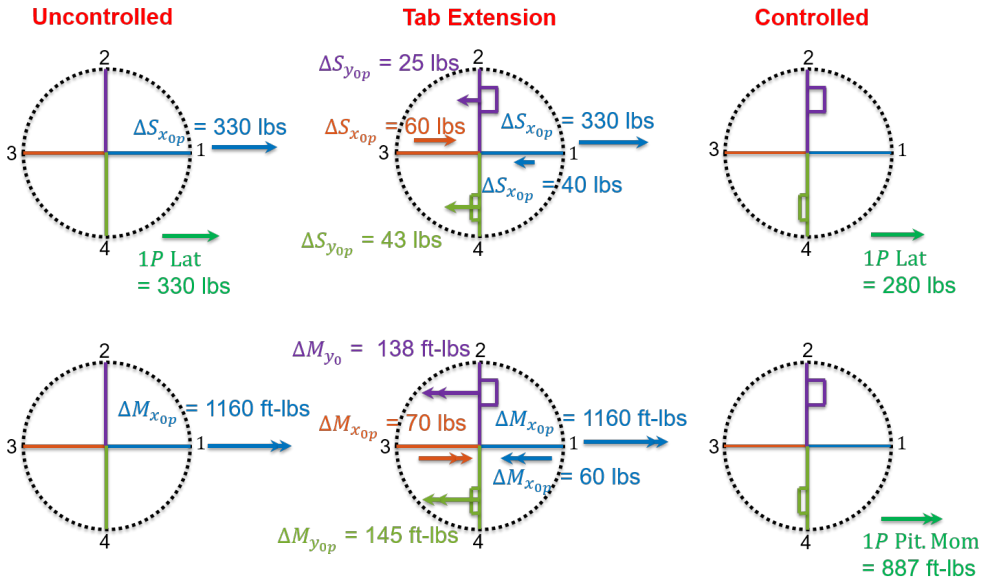

Fig. 17: Trailing-Edge Tab at 120 knots

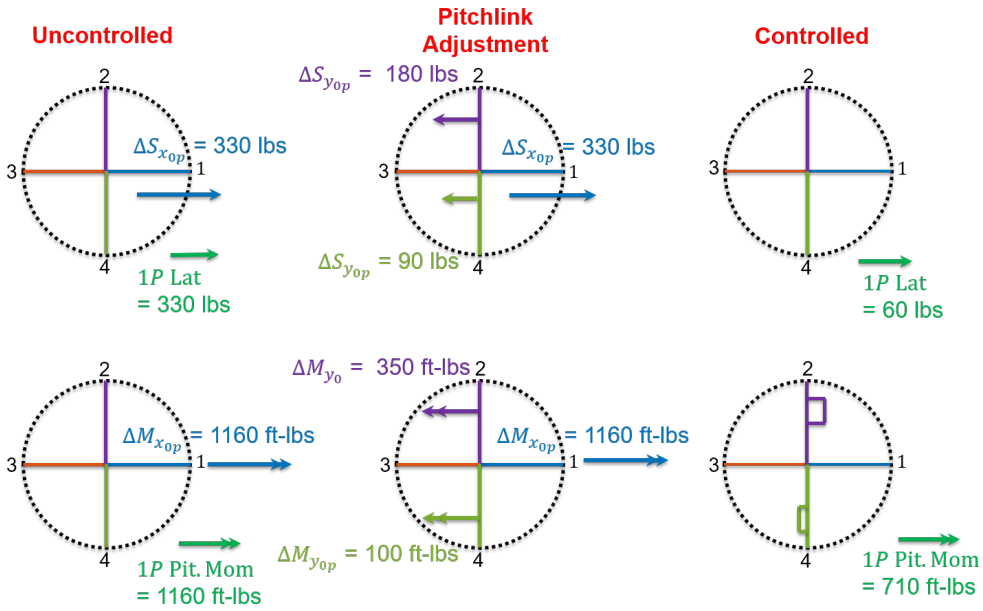

Fig. 18: Pitch link at 120 knots

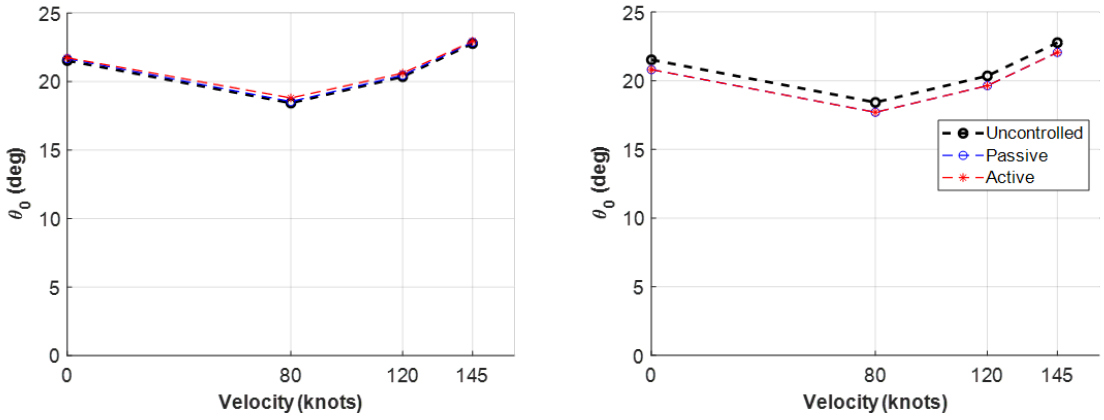

(a) Trim Collective Pitch - Tab

(b) Trim Collective Pitch - Pitch link

Fig. 19: Trim Collective Pitch over Airspeed Range

REFERENCES

[1]Rosen, A., Ben-Ari, R., "Mathematical Modelling of a Helicopter Rotor Track and Balance: Theory," *Journal of Sound and Vibration*, Vol. 200, (5), 1997, pp. 589–603.

[2]Bechhoefer, E., Power, D., "IMD HUMS Rotor Track and Balance Techniques," IEEE Aerospace Conference Proceedings, IEEEAC Paper No. 1191, Big Sky, Montana,, 2003.

[3]Berry, J.D., Branhof, R.W., Keller, J.A., Lem Grant, CW5., Grabill, P., "Investigation of Automated Rotor Smoothing Using Continuous Vibration Measurements," Proceedings of the American Helicopter Society 60^{th} Annual Forum, Baltimore, MD, June 7-10, 2004.

[4]Branhof, R.W., Keller, J.A., Lem Grant, CW5., Grabill, P., "Application of Automated Rotor Smoothing Using Continuous Vibration Measurements," Proceedings of the American Helicopter Society 61^{st} Annual Forum, Grapevine, TX, June 1-3, 2005.

[5]Epps, J. J. and Chopra, I., "In-flight tracking of helicopter rotor blades using shape memory alloy actuators," *Smart Materials and Structures*, Vol. 10, (1), 2001, pp. 104.

[6]Kennedy, D.K., Straub, F.K., Schetky, L.McD., Chaudhry, Z., Roznoy, R., "Development of an SMA Actuator for In-Flight Rotor Blade Tracking," *Journal of Intelligent Material Systems and Structures*, Vol. 15, (4), April 2004, pp. 235–248.

[7]Lengyel, A., van Schoor, M., Centolanza, L., Wilson, M., "Active Trim Tab for Rotor Track and Balance," Proceedings of the AHS Aeromechanics Specialist's Conference, San Francisco, CA, Jan. 23-25, 2008.

[8]Matalanis, C.G., Kuczek, A., Lin, R-S., Manes, E., Wake, B.E., Yeh, J., Chaudhry, Z., Brewer, P., "Development of an Active Trim Tab System for Onboard Rotor Tracking," Proceedings of the 66^{th} AHS International Forum and Technology Display, Phoenix, AZ, May 11-13, 2010.

[9]Norman T.R., Theodore, C., Shinoda, P., Fuerst, D., Arnold, U.T.P., Makinen, S., Lorber, P., O'Neill, J., "Full-Scale Wind Tunnel Test of a UH-60 Individual Blade Control System For Performance Improvement And Vibration, Loads, and Noise Control," Proceedings of the American Helicopter Society 65^{th} Annual Forum, Grapevine, TX, May 27-29, 2009.

[10]Fuerst, D., Arnold, U.T.P., Graham, D., "In-Flight Tuning: Wind Tunnel Test Results and Flight Test Preparation," Proceedings of the 67^{th} AHS Annual Forum, Virginia Beach, VA, May 3-5, 2011.

[11]Arnold, U.T.P., Fuerst, D., Hartmann, S., Hausberg, A., "Flight Testing of an In-Flight Tuning System on a CH-53G Helicopter," Proceedings of the 70^{th} AHS Annual Forum, Montreal, Quebec, Canada, May 20-22, 2014.

[12]Leon, O., Hayden, E., and Gandhi, F., "Rotorcraft Operating Envelope Expansion Using Extendable Chord Sections," Proceedings of the 65^{th} AHS International Forum and Technology Display, Grapevine, TX, May 27-29, 2009.

[13]Khoshlahjeh, M., and Gandhi, F., "Extendable Chord Rotors for Helicopter Envelope Expansion and Performance Improvement," *Journal of the American Helicopter Society*, Vol. 59, (1), January 2014.
doi: 10.4050/JAHS.59.012007

[14]Barbarino, S., Gandhi, F., and Webster, S., "Design of Extendable Chord Sections for Morphing Helicopter Rotor Blades," *Journal of Intelligent Material Systems and Structures*, Vol. 22, (9), June 2011, pp. 891–905.
doi: 10.1177/1045389X11414077

[15]Gandhi, F., and Hayden, E., "Design, Development, and Hover Testing of a Helicopter Rotor Blade Chord Extension Morphing System," *Smart Materials and Structures*, Vol. 24, (3), 2015.
doi: 10.1088/09645-1726/24/3/035024

[16]Moser, P., Barbarino, S., and Gandhi, F., "Helicopter Rotor-Blade Chord Extension Morphing Using a Centrifugally Actuated Von Mises Truss," *Journal of Aircraft*, Vol. 5, (5), 2014, pp. 1422–1431.
doi: 10.2514/1.C032299

[17]Krishnamurthi, J., and Gandhi, F., "Flight Simulation and Control of a Helicopter Undergoing Rotor Chord Extension Morphing," Proceedings of the 72^{nd} AHS Annual Forum, West Palm Beach, FL, May 17-19, 2016.

[18]Saberi, H., Khoshlahjeh, M., Ormiston, R., and Rutkowski, M., "Overview of RCAS and Application to Advanced Rotorcraft Problems," AHS Fourth Decennial Specialists Conference on Aeromechanics, San Francisco, CA, January, 2004.

[19]Hopkins, A.S., and Ormison, R.A., "An Examination of Selected Problems in Rotor Blade Structural Mechanics and Dynamics," Proceedings of 59^{th} American Helicopter Society Annual Forum, Phoenix, AZ, May 6-8, 2003.

[20]Peters, D.A., and He, C.J., "Correlation of Measured Induced Velocities with a Finite-State Wake Model," *Journal of the American Helicopter Society*, Vol. 36, (3), July 1991, pp. 59–70.

[21]Bae, E.-S., and Gandhi, F., "CFD Analysis of High-Lift Devices on the SC-1094R8 Airfoil," American Helicopter Society 67^{th} Annual Forum Proceedings, Virginia Beach, VA, May 3-5, 2011.